One-dimensional dynamic modeling and validation of maintenance-free lead-acid batteries emphasizing temperature effects

Kevin Siniard, Meng Xiao, Song-Yul Choe*

Mechanical Engineering Department, Auburn University, Auburn, AL 36848, USA

ARTICLE INFO

ABSTRACT

Lead acid batteries are still widely used for SLI (Starting–Lighting–Ignition) systems in vehicles because of the cost advantage. The batteries are frequently charged and discharged under different operation conditions, which continuously changes distribution of inner temperature of batteries. Variation of the temperature distributions significantly affects performance and durability of the battery. We developed a one-dimensional dynamic model based on the first principle of thermal dynamics and electrochemistry. The thermal model incorporates control volumes for each of the major constituents of the battery cells that is casing, electrolyte, and electrodes. The model was extended for a six-cell battery and used to analyze effects of discharging currents on the performances and temperature, compared with results from a three-dimensional finite element analysis and tested against experimental results obtained from a thermal chamber and using thermal imaging.

1. Introduction

Advancements in automotive battery technology from electrode and electrolyte materials to a range of environmental effects on battery performance have been the leading focus for researchers in recent years. There have been a number of approaches implemented to characterize battery performance for traditional internal combustion vehicles and hybrid battery applications. The life span and performance of batteries specifically SLI (Starting–Lighting–Ignition) lead acid batteries have been well documented by researchers [2–9].

Several researchers have incorporated complicated equivalent circuits to represent the various components of the battery. While the equivalent circuit approach provides a basic estimation of the inner workings of the battery, the electrochemical processes that are the backbone of the battery are neglected. For instance, equivalent circuit methods provide effective surface area values as a mere function of the SOC [10]. In reality, electrode effective surface area is a product of the material porosity, reaction rate and the electrode–electrolyte interface, temperature, diffusion rate, and electrolyte concentration. Due to the complexity of the chemical reactions and transport of ions across the electrolyte reservoir a one-dimensional model can provide concentration of ions, temperature, reaction rate, and phase potentials of the battery cell that will be more comprehensive than those approximated by the electrical circuit components.

Esperilla and Felez addressed the thermal effects on lead acid batteries in terms of thermodynamic equations along with an equivalent circuit to represent the electrochemical reaction of the battery cells [3]. An alternative method, presented by Gu et al., uses a Thevenin equivalent model focusing on battery electrochemistry by considering activity of the migrating ions and porosity of electrodes to obtain a more comprehensive model of the battery during charge and discharge [5]. Kim and Hong focused on effects of varying battery parameters on the electrolyte concentration and discharge performance neglecting temperature change. Additionally, close attention was paid to the effects of the limiting current density [9]. These models concentrate on specific aspects of automotive batteries, but do not completely describe behaviors of a six cell battery dynamics and performance.

Therefore, the approach outlined in this paper includes various aspects of previously mentioned models as well as a few novel techniques to represent the battery's physical properties and performance. Accepted electrochemical, thermodynamic, and heat transfer methods are employed as the equivalent circuit does not adequately represent complex battery electrochemistry and mass transport. Effects of temperature and heat generation focus mostly on the discharge process when high current is present.

2. Mathematical descriptions

Dynamic characteristics of a lead acid battery depend on several parameters that are constantly changing. The complexity of the

* Corresponding author at: Mechanical Engineering Department, 202 Ross Hall, Auburn University, Auburn, AL 36848, USA. Tel.: +1 344 844 3382; fax: +1 334 844 3307.

E-mail address: choe@auburn.edu (S.-Y. Choe).

Nomenclature

a	specific surface area for electrode (cm^{-1})
c_p	specific heat $(J\,kg^{-1}\,K^{-1})$
C	concentration $(mol\,cm^{-3})$
D	diffusion coefficient $(cm^2\,s^{-1})$
E_j	open circuit potential (V)
F	Faraday's constant $(96,487\,C\,mol^{-1})$
h	heat transfer coefficient $(W\,cm^{-2}\,K^{-1})$
H	enthalpy (J)
i_0	reference exchange current density $(A\,cm^{-2})$
I	applied current density $(A\,cm^{-2})$
j	transfer current density $(A\,cm^{-2})$
k	thermal conductivity $(W\,m^{-1}\,K^{-1})$
q	volumetric heat generation rate $(W\,cm^{-3})$
Q	state of charge (SOC)
R	universal gas constant $(8.3143\,J\,mol^{-1}\,K^{-1})$
S	partial molar entropy $(J\,mol^{-1}\,K^{-1})$
t^0_+	transference number
T	cell temperature (K)
V_c	cell volume (cm^3)

Greek symbols

α	transfer coefficient
δ	exchange current density correction factor
ε	porosity of a porous medium
γ	activity coefficient
φ	potential in a phase (V)
η	surface overpotential (V)
κ	ionic conductivity of electrolyte $(S\,cm^{-1})$
κ_D	diffusional conductivity $(A\,cm^{-1})$
ρ	density $(g\,cm^{-3})$
σ	conductivity of solid active material $(S\,cm^{-1})$
υ	stoichiometric coefficient
ζ	area correction factor

Subscripts

a	anode reaction
b	battery
c	cathode reaction
e	electrolyte phase
eff	effective
int	internal
irr	irreversible
j	grid number
n	electrode reaction, Pb, PbO_2
rev	reversible
s	solid phase
t	charge transfer

internal chemical reactions of the battery requires a few assumptions in order to appropriately model battery performance. The relationships governing the battery performance are based on the following assumptions [11]:
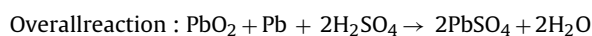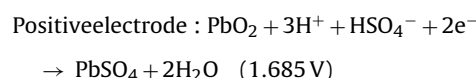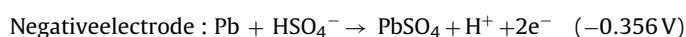
(a) The lead acid cell is comprised of a lead dioxide electrode, PbO_2, an electrolyte, reservoir, a porous separator and a lead electrode, Pb.
(b) The electrode surface area is constant in the direction along the electrode surfaces and the associated electrolyte concentration is constant.
(c) The electrolyte is completely dissociated into H^+ and HSO_4^- ions and no recombination occurs.
(d) The initial temperature of the battery is 300 K.

(e) The model is one-dimensional in the direction perpendicular to the electrodes, and
(f) No gasses are produced during reactions.
(g) Overcharge is not considered.

The flow chart shown in Fig. 1, from left to right, presents the specified input values and initial conditions, governing equations, and outputs. The physical equations used for the modeling are the Nernst equation, the Butler–Volmer equation, combined with the energy conservation, material balance, and Darcy's equations that characterize the dynamic physical and chemical properties of the battery during the charge and discharge processes.

2.1. Cell voltage

The reaction shows the chemistry of the lead-acid battery at discharge. The reversible process will move in the opposite direction when charging

$$Negative\,electrode : Pb + HSO_4^- \rightarrow PbSO_4 + H^+ + 2e^- \quad (-0.356\,V)$$

$$Positive\,electrode : PbO_2 + 3H^+ + HSO_4^- + 2e^-$$
$$\rightarrow PbSO_4 + 2H_2O \quad (1.685\,V)$$

$$Overall\,reaction : PbO_2 + Pb + 2H_2SO_4 \rightarrow 2PbSO_4 + 2H_2O$$

When under no load conditions the battery settles at a chemical equilibrium, but due to the opposing charges an electric potential is created. Prior to current flow experienced during charge or discharge, the battery has an initial electromotive force, EMF, that is described by the difference in the electrode potentials as follows:

$$E = E_c - E_a \tag{1}$$

where E_c and E_a and are the potentials of the cathode and anode, respectively [6]. For the chemical reaction described above, the standard potential of a cell, E°, is derived from the change of Gibbs free energy. The dependence of cell potential on acid concentration when no current is flowing is governed by the Nernst equation:

$$E = E^\circ - \frac{R \cdot T}{n \cdot F} \ln \prod_{n=1}^{\infty} (m_i \gamma_i)^\upsilon \tag{2}$$

where R is the gas constant, T is temperature, m is molality (acid concentration), γ is activity coefficient, and υ is the stoichiometric coefficient.

Several values for the electrode potentials at various concentrations found through experimental process are provided by reference materials [1]. The activity coefficient is electrolyte concentration dependent and is a combination of the negative and positive ions involved in the reaction and cannot be individually calculated [5]. For the purposes of modeling, the activity coefficient is found as a function of molality by curve fitting to the reference data [1]. The stoichiometric coefficient is taken from the chemical reactions described above.

When charge or discharge current is applied, overpotentials, η, are formed. Considered overpotentials are those that occur as a result of charge transfer during chemical reactions, ohmic losses, and diffusion of ions across the electrolyte. Specifically, overpotential is calculated as the difference in solid phase and electrolyte phase potentials compared to the equilibrium potential.

$$\eta = \phi_s - \phi_e - E_{Pb} \text{ for negative electrode and}$$
$$\eta = \phi_s - \phi_e - E_{PbO_2} \text{ for positive electrode} \tag{3}$$
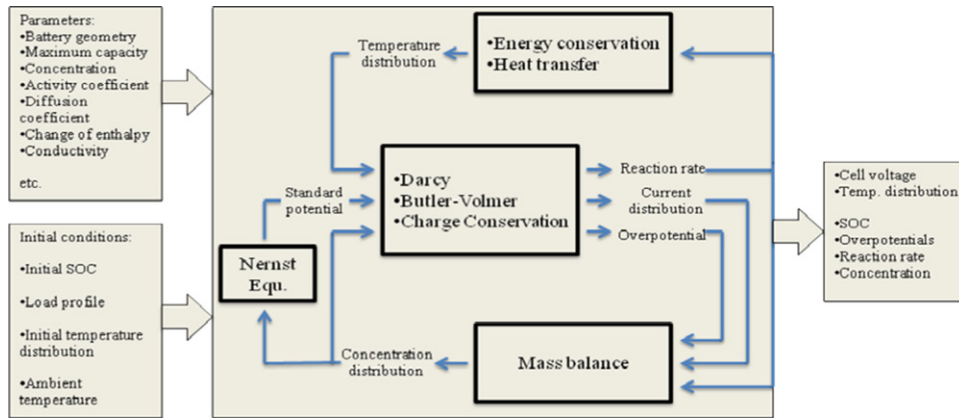
Fig. 1. Modeling flow chart.

where ϕ_s is the potential of the electrode solid phase, ϕ_e is the potential of the electrolyte phase, E_{Pb} and E_{PbO_2} is the equilibrium potentials of the negative and positive electrode[6].

The overpotential occurs by charge transfer at the battery electrodes and is governed by the Butler–Volmer equation [3] that is simplified.

For large overpotential at the anode and cathode, η_t, is calculated using:

$$\eta_t = \frac{R \cdot T}{z \cdot \alpha \cdot F} \ln \frac{i}{i_0} \quad \text{or} \quad \frac{R \cdot T}{z \cdot (1-\alpha) \cdot F} \ln \frac{i_0}{i} \tag{4}$$

For small overpotential at the anode and cathode [7], the equation above can be simplified further and approximated with a linear function, $\eta_t = RTi/i_0F$.

When the battery experiences current flow, the concentration gradient is not equal to zero and the electrolyte concentration changes. As a result, diffusion overpotential is created:

$$\eta_d = \frac{R \cdot T}{n \cdot F} \cdot \ln \Pi \left(1 - \frac{i}{i_L}\right)^\nu \tag{5}$$

If the activity of the ions formed increases due to the chemical reaction, the diffusion gradient is directed away from the electrode where the reaction took place. The limiting current density is a function of the activity of the electrolyte, the diffusion coefficient, and diffusion layer thickness [1]:

$$i_L = \frac{z \cdot F \cdot D \cdot \gamma}{\delta} \quad \text{and} \quad \delta = \frac{2}{\sqrt{\pi}} \cdot \sqrt{D \cdot t} \tag{6}$$

where D is the diffusion coefficient, t is time, z is number of electrons transferred, F is Faraday's constant, γ is the activity, and δ is the diffusion layer thickness.

The diffusion coefficient is concentration and temperature dependent and is found by curve fitting to experimental values taken for various concentrations, C and temperature, T shown below [9]. When the temperature is equal to the specified room temperature, 300 K, the exponential term becomes unity.

$$D = \exp\left[\frac{2174.0}{298.15} - \frac{2174.0}{T}\right] \cdot (1.75 + 260.0 \cdot C_e) \cdot 10^{-5} \tag{7}$$

Finally, the cell voltage is described by considering all of overpotentials at each electrode. The overpotentials at the anode and cathode are denoted by subscripts a and c, respectively

$$E = E^0 + (\eta_t + \eta_d)_a - (\eta_t + \eta_d)_c - I \cdot R_{int} \tag{8}$$

where I, current, represents the current flowing through the cell calculated as the product of the electrode current density and surface area and R_{int} is the resistance of the separator and electrolyte [1].

2.2. Conservation of charge

Current flowing through the electrolyte phase of the positive electrode is driven by electric potential and the varying concentrations near the electrode/electrolyte interface. Transport of ions and flow of electrons are vital processes in battery process, and the conductivity of the active materials determines the rate of that flow. Quantifying the ionic electrolyte conductivity, as with the diffusion coefficient, requires calculations as a function of electrolyte concentration and temperature [9].

$$\kappa = C_e \cdot \exp\left[1.1104 + (199.475 - 16097.781 \cdot C_e)C_e \right.$$
$$\left. + (3916.95 - 99406.0C_e - 721960/T)/T\right] \tag{9}$$

Ionic conductivity, calculated above, is employed to determine effective ionic conductivity, κ^{eff}, incorporating porosity effects and diffusional conductivity, κ_D^{eff}, describing transference effects.

$$\kappa_{eff} = \kappa \cdot \varepsilon^{1.5} \tag{10}$$

$$\kappa_D^{eff} = \frac{R \cdot T \cdot \kappa^{eff}}{F} \cdot (2 \cdot t_+^0 - 1) \tag{11}$$

where t_+^0 is the transference number, which refers to each set of ions contribution to the overall current [6]. Involved in the charge transport of the ions in the electrolyte mixture, the transference number is unique to each chemical reaction. The overall transference number, derived from experimental data, refers to the transference of the hydrogen ion [12]. The result of the forces in liquid phase on the system is described by the conservation of charge equation;

$$\frac{\partial}{\partial x}\left(\kappa^{eff} \cdot \frac{\partial}{\partial x}\phi_e\right) + \frac{\partial}{\partial x}\left[\kappa^{eff} \cdot \frac{\partial}{\partial x}(\ln C)\right] + a_n \cdot i_n = 0 \tag{12}$$

where i_n is the current density in the electrolyte or solid phase, ϕ_e is the electrolyte potential, C is the concentration of the electrolyte, a_n is the active area, κ^{eff} is the effective electrolyte conductivity, while κ_D^{eff} includes tortuosity effects.

2.3. Material balance

While the conservation of charge equation describes the reaction rate at the electrodes, the material balance equation illustrates the chemical processes across the entire battery cell. Material balance is a function of the concentration of the ions that make up the electrolyte as well as the diffusion caused by the concentration gradient of those ions. Furthermore, the electrolyte fills spaces of the porous electrodes, therefore the porosity of the electrodes

must be considered. The effective diffusion coefficient, D_{eff}, is calculated using the equation below, where the diffusion coefficient, D, is found using Eq. (7)

$$D^{eff} = D \cdot \varepsilon^{\zeta} \tag{13}$$

The overall material balance equation is

$$\frac{\partial}{\partial t}(\varepsilon_e \cdot C) = \frac{\partial}{\partial x}\left(D^{eff} \cdot \frac{\partial}{\partial x}C\right) + \frac{(3 - 2 \cdot t_+^0)}{2F} \cdot a_n \cdot i_n \tag{14}$$

where ε is porosity [6].

The conservation of species equation above removes the effects of momentum outlined in the models [6]. Momentum conservation that is a function of electrolyte saturation, only exhibits significant effects during overcharge, therefore is neglected in this study.

As the rate of reaction directly changes the current density, the concentration is also affected. In addition, as the concentration and current density is affected, the diffusion coefficient changes, altering the diffusion rate of the ions across the electrolyte reservoir. Consequently, the reaction rate determined by the Butler–Volmer equation directly and indirectly effects each parameter described in conservation of species.

Further examination of the Butler–Volmer, material balance, conservation of charge and species equations lead to a number of model simplifications. The first vital value is the overpotential. There is a solid phase potential, ϕ_s, and electrolyte phase potential, ϕ_e, for each point across the battery cell. Comparison with the equilibrium potential, E, provides the overpotential or difference between equilibrium and actual battery potential. The equilibrium potential for each electrode at various electrolyte concentrations is provided by curve fitting to the tabular values that result in the following relationship for the electrodes potentials to electrolyte concentration [1]:

$$E_-(c) = -0.0002C^5 + 0.0032C^4 - 0.0224C^3$$
$$+0.0725C^2 - 0.1267C - 0.2226 \tag{15}$$

$$E_+(c) = 0.0002C^5 - 0.0034C^4 + 0.024C^3 - 0.0759C^2$$
$$+0.1303C + 1.55 \tag{16}$$

On the other hand, the values of overpotential will remain in the linear portion for normal battery operating conditions with errors of only .02–.04 V for overpotential values up to .4 V. After the Butler–Volmer equation is linearized, the conservation of charge equation is substituted. This simplification of the equations also creates a more timely convergence of the equations for each cell division [5]:

$$\frac{\partial}{\partial x}\left(\kappa^{eff} \cdot \frac{\partial}{\partial x}\phi_e\right) + \frac{\partial}{\partial x}\left[\kappa^{eff} \cdot \frac{\partial}{\partial x}(\ln C)\right] + a_n \cdot i_n = 0 \tag{17}$$

where

$$j_H = a_n \cdot i_n = i_0 \cdot \left(\frac{C_e}{C_{e.\max}}\right)^{\gamma} \cdot \left(\frac{\alpha_a + \alpha_c}{RT}F\right)(\phi_s - \phi_e - E_j) \tag{18}$$

Due to the slowly changing acid concentration, initially the second term in the conservation of charge equation is taken as constant. Therefore, the concentration and temperature at a given time is used to calculate κ^{eff} and κ_D^{eff}. Now that the overpotential equation is simplified and other values are assumed constant, the only unknown variables remaining are the phase potentials. The conservation of charge for the electrolyte is valid across the entire battery cell, resulting in the same number of equations as cell divisions. However, the solid phase conservation of charge refers to only the

battery electrodes and is a function of effective conductivity, solid phase potential and reaction rate [6]:

$$\frac{\partial}{\partial x}\left(\sigma^{eff} \cdot \frac{\partial}{\partial x}\phi_e\right) - a_n \cdot i_n = 0 \tag{19}$$

The entire battery cell is divided into one hundred grids with 26 assigned to the negative electrode and 37 to the positive electrode resulting in a total of 163 equations representing the conservation of charge. MATLAB solves the system of equations resulting in solid phase potentials at the electrodes and the electrolyte phase potential across the battery cell. Employing the resulting phase and equilibrium potentials provides overpotential at each section across the cell. Overpotential is then used to calculate the reaction rate, j_H, by means of the Butler–Volmer equation [5].

Convergence of the conservation of charge for the electrolyte and solid electrodes equations provides the inputs for the conservation of species equation. Using the reaction rate calculated from the initial acid concentration, the conservation of species equation is employed to determine the change in concentration with each time step. Similar to the method used for calculation of reaction rate, an equation for each segment or grid of the battery cell is derived. While the initial values are known, the acid concentration as a function of the change in time provides the variables for the equation. The battery cell is divided into one hundred segments, and the same number of equations represents each section. Solving the system of equations provides the acid concentration gradient across the cell.

3. Energy conservation

During the charge and discharge processes of a lead acid storage battery, there is a large amount of energy transfer through the battery materials. As a result, during operation, battery internal temperature cannot be assumed constant and number of processes affects the amount of energy released or transferred. The total change of Gibbs free energy is equal to the change in enthalpy of the system minus the product of the temperature and change of entropy for constant temperature applications. However, the simplified constant temperature calculation is not suitable for high current battery applications. The Maxwell thermodynamic relation provides a substitution for the enthalpy terms and results in the overall Gibbs free energy equation in terms of measurable properties temperature, pressure, and specific volume, where dP and dQ_t are negligible because of constant internal pressure assumed [6]:

$$dG = -S_{rev}dT + V \cdot dP + E \cdot dQ_t \tag{20}$$

In order to fully encompass the causes for temperature change within the system, the effects of reversible and irreversible processes are considered. The entropy of the reversible process, where there is no entropy generation, is found using the following equation where the temperature coefficient, $\partial E/\partial T$, of the active materials is specified in several reference materials [1,2]. The temperature coefficient refers to the effect of temperature on cell potential. If cell potential increases as temperature increases, the coefficient is positive and vice versa.

For the irreversible processes, there is entropy generation, where energy is dissipated from the previously mentioned overpotentials. The amount of heat generated is the product of the overall current, and the total overpotential including ohmic, diffusion, and charge transfer discussed above [7].

Heat transfer between the battery components and the external environment is considered using the method of equivalent resistance. The equivalent resistance is a function of the thermal conductivity, surface area and heat transfer coefficient. The plastic battery casing has a thermal conductivity of $0.2\,\mathrm{W\,m^{-1}\,K}$. The

thickness and surface area are calculated depending on battery dimensions. The third term of Eq. (21) provides the heat transfer rate between the external environment and the internal components of the battery [3].

The overall aforementioned facts describing the energy in the system are included:

$$m \cdot c_v \cdot \frac{dT}{dt} = Q_t \cdot \left(\frac{dE}{dT}\right) \cdot T + \eta \cdot I - \frac{1}{R_{eq}} \cdot (T_a - T) \tag{21}$$

where T_a is the ambient temperature, and T is the internal temperature of the battery. The value for specific heat capacity, c_v, changes with the concentration of the electrolyte solution that is constantly changing during the charge and discharge processes. The values for specific heat capacity at various concentrations are provided in Ref. [1]. By fitting a curve to the tabular values as a function of molality (concentration), the value for specific heat capacity is calculated.

As shown in Eq. (21), cell temperature is function of various chemical properties and transient battery parameters. The heat generation terms caused by overpotential and the temperature coefficient must be quantified for each cell individually. Therefore, the heat generation at the each electrode is the sum of the values across the entire volume. The sum of two heat generation rate terms at each electrode is rewritten as [7]:

$$q = \frac{1}{V_c} \int_{V_c} \sum_j a_n \cdot i_n \cdot \left(\eta - T \cdot \frac{\partial E_j}{\partial T}\right) \tag{22}$$

The total cell volume is denoted as V_c. Using the equivalent resistance method to calculate the R_{eq} mentioned above a temperature profile is established for the casing, electrode and electrolyte [3]. Employing the equation above provides heat generation rate in units of $W\,m^{-3}$ and is applied over the cell volume.

4. Simulation and analysis

4.1. Numerical procedures

The finite difference method is employed in order to approximate the partial derivatives of the various governing equations outlined in the sections above. Initially, the method calls for division of the domain in question into a uniform grid. For our purposes, a single battery cell is divided into a specified number of equal segments, Δx, for a total number of one hundred grids. Specified by the battery dimensions, the positive electrode, negative electrode, electrolyte reservoir consists of 36, 27, and 37 grids, respectively. Utilizing finite difference approximation, the partial derivative of phase potential with respect to x can be rewritten using the central difference method [13]. The computer modeling efforts aim to fully represent battery performance under various discharge, charge, and temperature ranges. However, performance is dependent on complex electrochemical processes that determine electrolyte concentration, reaction rate, conductivity, etc. In order to recognize the causes of inconsistent response under varied conditions, researchers must first examine the response of these complex processes.

As with any dynamic system, initial and boundary conditions are necessary to initiate and close the mathematical modeling. Previously mentioned equilibrium potentials are set to provide an initial battery voltage. Similarly, electrolyte concentration, cell temperature, and initial current density are specified parameters. The first area of consideration is current density of the battery components. The initial current experienced by the current collectors is defined as:

$$-\sigma_{eff} \cdot \frac{\partial \phi_s}{\partial t}\bigg|_{x=0} = -\sigma_{eff} \cdot \frac{\partial \phi_s}{\partial t}\bigg|_{x=L} = \frac{I}{A} \tag{23}$$

for a given current density, while everywhere else on the cell boundary is defined as:

$$\frac{\partial \phi_e}{\partial t}\bigg|_{x=0} = -\sigma_{eff} \cdot \frac{\partial \phi_e}{\partial t}\bigg|_{x=L} = 0 \tag{24}$$

The initial conditions of various battery parameters are determined as a function of initial electrolyte concentration. Therefore, initial electrolyte concentration at the boundaries is of great concern. First, the initial concentration is equal to the concentration prior to load and there is no gradient at the boundaries of the electrodes and current collectors [6]:

$$c_{e,initial} = c_0, \quad \frac{\partial \phi_e}{\partial t}\bigg|_{x=0} = -\sigma_{eff} \cdot \frac{\partial \phi_e}{\partial t}\bigg|_{x=L} = 0 \tag{25}$$

Furthermore, there is no electrolyte flow prior to current flow through the battery, so the change in electrolyte concentration at the boundaries is shown above to equal zero. As outlined in Section 1, thermal effects on the dynamic performance of the battery are the main focus of the research. The initial cell temperature is set to 300 K, but is altered with the introduction of varying ambient temperatures:

$$-\kappa \cdot \frac{\partial T}{\partial x} = h \cdot (T_a - T) \tag{26}$$

where k is thermal conductivity of the outer casing, h is the overall convective heat transfer coefficient.

4.2. Analysis under isothermal condition

Prior to the investigation of transient temperature effects on battery performance, an intense investigation into response of reaction rate, overpotential, and porosity including their effects on electrolyte concentration and cell voltage was performed. The load or supply current is considered the major factor determining battery kinetics and the rate of chemical processes.

4.2.1. Overpotential and reaction rate

Overpotential and reaction rate are identified as the most critical parameters for accurate representation of battery performance. Specifically, overpotential for each electrode grid determines the frequency and reaction rate, at which the chemical reactions take place. As the overpotential at that point increases, so does the reaction rate. While the magnitude of reaction is heavily dependent on the overpotential, the electrode effective surface area plays a significant role. Surface area is constantly changing as active materials are depleted while the electrodes become increasingly or decreasingly porous depending on the process and are calculated using the ratio of available capacity to maximum capacity.

The exchange current density has a similar response, but is proportional to electrolyte concentration is shown [3]:

$$i_n = i_{n,\max} \cdot \left(\frac{c_e}{c_{e,\max}}\right)^{\delta} \tag{27}$$

The correction factor, δ, is .3 and 0 for the positive and negative electrodes, respectively. Therefore, the negative electrode current density remains constant regardless of electrolyte concentration. Conversely, the positive electrode current density increases during charge as the concentration approaches the maximum and decreases during discharge in Fig. 3.

Investigation of modeling results show temperature of the battery environment and current applied or drawn from the battery exhibit significant effects on the reaction rate. As expected, when the current is increased, the reaction rate speeds up to accommodate. There is also a considerable gradient created across the electrodes as more reactions occur at the electrode/electrolyte
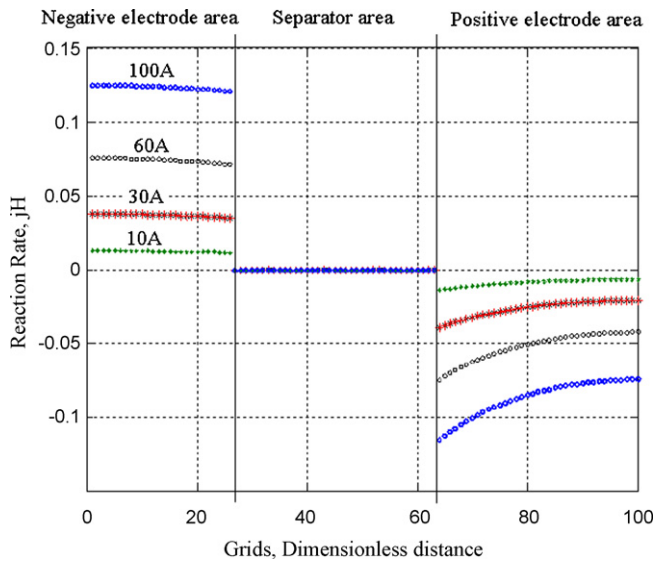
Fig. 2. Isothermal reaction rate, A cm^{-3}, after 15 min discharge at 10 A (.), 30 A (*), 60 A (o), 100 A (o).

Fig. 3. Reaction rate of the positive electrode after 15 min discharge at 30 A and 280 K (solid), 300 K (dash), 340 K (solid dot), and 380 K (dash dot).

interface increasing with current as shown in Fig. 2. The reaction rate across the negative electrode is relatively uniform as the current density remains constant over the entire range of concentrations. However, the positive electrode reveals a steeper gradient due to the current density dependence on concentration illustrated by Eq. (30).

While applied current has a considerable effect on performance, everything from the electrolyte conductivity to reaction and diffusion rates is a function of temperature. Therefore, variation in temperature affects the amount and location of the chemical reactions during battery operation. On the molecular level, temperature increase causes a rise in particle collision leading to a rise in reactions across the cell.

4.2.2. Electrolyte concentration

Initially under equilibrium conditions, the electrolyte concentration is assumed constant across the battery cell. During charge or discharge process, ions diffuse towards and away from the electrodes to react at the electrode area/separator area interface. Ion diffusion along with continuous chemical process causes differing electrolyte concentration across the battery cell. Various parameters, mostly determined by charge or discharge current and temperature, greatly affect the degree of concentration change [9].

As the battery is discharged, the electrolyte concentration decreases at a rate determined by the load applied. However, constant current does not expend the electrolyte at a constant rate, as the reaction rate is constantly changing due to a number of factors. Fig. 4 shows acid concentration across the battery cell following fifteen minutes of continuous discharge at 10 A, 30 A, 60 A, and 100 A at room temperature, 300 K. For each case, the battery is initially at full charge with a uniform acid concentration of 5.6 mol cm^{-3}.

During discharge, as the electrochemical processes occur, the electrodes react with the electrolyte decreasing the overall amount of electrolyte present as water takes place of the displaced sulfuric acid. Non-uniform concentration occurs for a number of reasons. The porosity of the electrodes is determined by the electrode material properties and chemical reactions continuously altering the structure, specifically surface area, and chemical makeup of the electrode interface. Inconsistency of effective surface area, effective current density, and reaction rates at the interface results in a significant slope as shown below. The electrolyte concentration
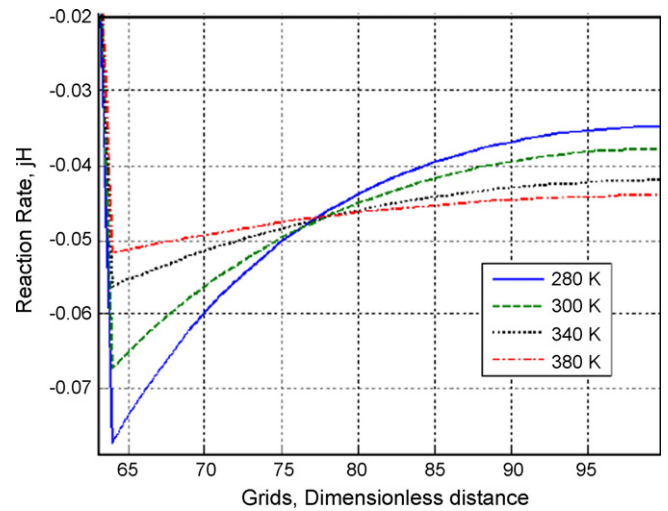
grows increasingly uniform as temperature rises consistent with the reaction rate shown in Fig. 2.

These findings are consistent with the profile provided in Fig. 3 showing a greater number of reactions at the electrode area/separator area interface. Consequently, the minimum acid concentration occurs at the positive electrode boundary where the least amount of reactions takes place. While the magnitude of current determines the gradient, the average acid concentration is more affected by the battery SOC than the current drawn from the battery. Additionally, the load current directly influences the reaction rates and SOC. In other words, acid concentration depends on the amount of time a battery is under a certain load as the gradient increases over time.

It is important to note that the minimum acid concentration always occurs at the positive electrode. As a result, during discharge the positive electrode controls the electrochemical performance. When the acid concentration at the positive electrode is completely depleted, the battery is considered fully discharged or SOC equal to zero [9]. However, during charge, when the current flows in the opposite direction, the gradient has the opposite slope where the minimum concentration occurs at the negative electrode. The figure on the left shows increasing gradient as a greater charge current is applied, consistent with discharge results. Furthermore, the temperature has similar effects on the concentration growing increasingly uniform as temperature rises from 280 K and 380 K as shown in Fig. 4.

Acid concentration directly determines the voltage experienced at the terminals under load as shown in Fig. 4, but also when no load is applied. The amount of voltage recovery is mostly determined by the load magnitude of the load removed from the battery. However, the electrolyte concentration slowly regains a uniform equilibrium state after the load is removed and the terminal voltage is affected. As the electrolyte concentration gradient decreases when a 50 A discharge load is removed and the battery is open. After 1000 s have passed a significant change in concentration occurs, and after 1500 s the electrolyte regains an equilibrium state.

4.2.3. Phase potentials

As expressed in the previous equations the electrolyte and solid phase potentials are directly determined by the electrochemical kinetics described by the material balance, charge balance, and Darcy equations. The matrix constructed using the finite difference approach converges in order to calculate the phase potentials across the cell. The electrolyte phase potential is a resultant of the
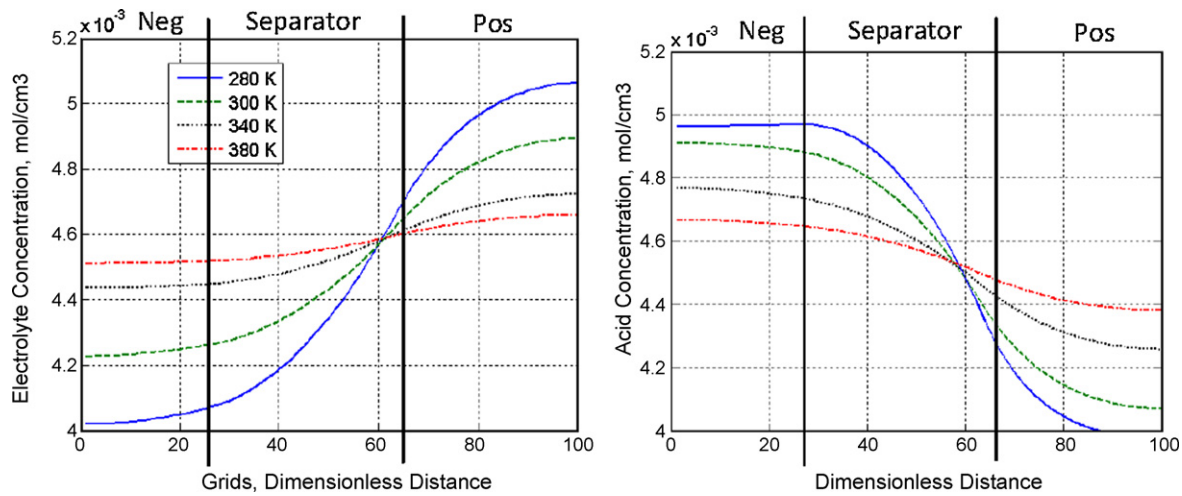
Fig. 4. Acid concentration gradient, mol cm^{-3}, after 15 min discharge at 60 A. (Right) discharge from full charge and (Left) charge from 50% SOC.

conservation of charge across the cell while the solid phase potential only occurs at the solid electrodes. Since the current collectors are attached at the electrode boundaries, the cell potential which is delivered to the battery terminals is determined by the solid phase potential at the point of contact between the electrodes and current collectors. The solid phase potential at the electrodes remains constant across the thickness of each.

The cell potential is a function of acid concentration at each electrode. As expected, the solid phase potential decreases for both electrodes during discharge as the concentration at each lessens causing a decrease in overall cell potential. When the concentration gradient arises the electrolyte phase potential experiences a significant gradient across the cell during the discharge process. This variation directly influences solid phase potential as the system of equations solves for each simultaneously. The negative electrode is specified as the reference electrode since the electrolyte phase potential at the boundary remains zero throughout the various processes.

4.3. Analysis under non-isothermal conditions

Initial thermal effects were derived using a simplified model neglecting the effects of heat generation and convection with a purely isothermal representation. The transient thermal model attempts to merely quantify the amount of energy generated, dissipated, and transferred between the battery components as a means to determine the average temperature of the cell in order to model battery performance. In addition, control volumes of the casing, positive and negative electrode, and electrolyte reservoir are implemented and constructed as a three-dimensional model investigating temperature distribution. For our purposes, the battery is first modeled as a closed system where no heat is lost or added to the system. Secondly, a non-adiabatic system is modeled using the same principles discussed in the previous section. The amount of heat generation is extracted from the MATLAB model and implemented during finite element analysis.

4.3.1. Acid concentration and terminal voltage

The temperature dependence of the governing equations causes a significant change in the reaction rate at the electrodes as shown in Fig. 3. As reaction rate grows increasingly uniform at high temperatures so does the concentration.

On the molecular level, the diffusion of ions and ionic conductivity of the electrolytes establish electrolyte concentration and both are a function of temperature. Increase in ionic conductivity allows

ions to move more freely through the medium, while the diffusion coefficient determines the speed at which ions diffuse to areas of lesser concentration. Ionic conductivity and diffusivity significantly increase as temperature rises leading to a lesser gradient during the charge and discharge processes.

The effects of temperature increase on the electrolyte concentration are evident for the three cases illustrated in Fig. 5. The adiabatic and non-adiabatic cases show an increase in temperature from the isothermal simulations leading to elevated electrolyte ionic conductivity and diffusion rates. Although increased temperatures act as a catalyst to chemical reactions, the batteries actually discharge slower as the lesser gradient aids in the battery's ability to hold charge or capacity.

As expected the highest temperatures occur during adiabatic process with no heat transfer to the external environment leading to lowest concentration gradient across the battery cell as shown in Fig. 5 as the amount of reactions near the interface is comparable to reactions within the porous cells. The lower concentration in certain areas is due to lower reaction rates and an increase in diffusion rate at higher temperatures. Although the difference in concentration between the three cases is evident, obvious effects to the discharge performance is only significant at high currents and extreme temperatures some time after the initial load is exerted. In
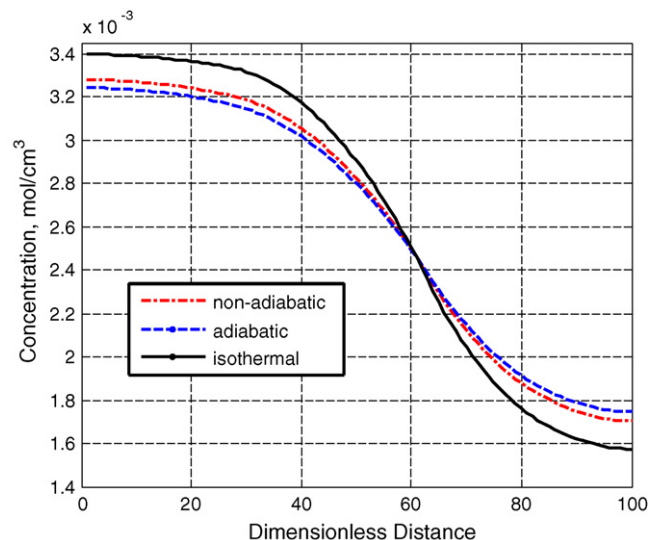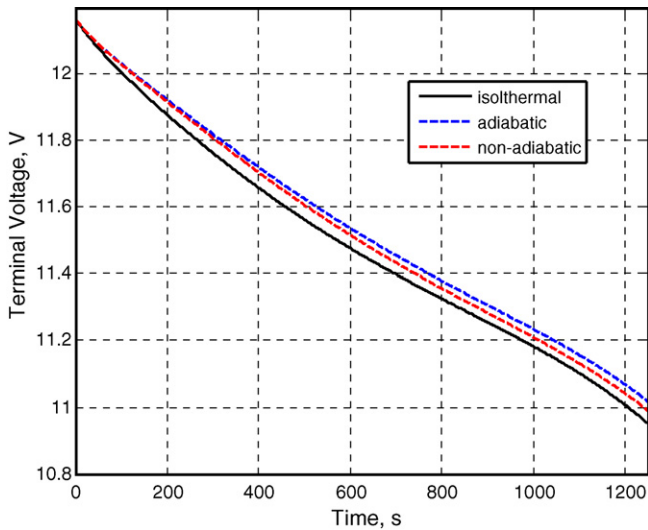

Fig. 5. Temperature effect on acid concentration.

Fig. 6. Temperature effects on terminal voltage at 100 A discharge.

Fig. 7. Temperature distribution for 60 A discharge after 3 min.

addition to transient effects, extreme temperatures high and low greatly affect the available capacity even at no load.

At elevated temperatures, chemical reactions take place at a greater rate, but also increase ionic conductivity and diffusion rates. This fact is illustrated by the isothermal, adiabatic, and non-adiabatic cases below. Initially, when the temperatures are relatively close, the discharge performance is similar. The discrepancy between the cases is caused by the temperature coefficient which determines cell voltage as a function of temperature. However, after 600 s as the temperatures continue to rise, there is a significant difference in terminal voltage. Near the end of discharge the voltage is .1 V more when compared to the isothermal case at 300 K.

The same effect holds true during charge as the temperature grows over time the cell voltage increases compared to the isothermal case, as shown in Fig. 6. However, due to low charge currents the amount of temperature change is not large enough until well after the initial supply current is applied to show a considerable change.

4.3.2. Comparison with three-dimensional finite element analysis

To fully encompass each component contribution to the system requires implementation of a three-dimensional model. The battery consists of six identical cells connected in series separated from one another by a thin plastic divide. The positive and negative electrodes are 12.6 cm × 14.3 cm with varying thickness depending on the cell design with the negative electrode designed slightly smaller. The electrodes are connected by the current collectors attached to the tab extending from each electrode in order to deliver or receive currents from the terminals. A 1.25 cm thick polyethylene outer casing protects the internal components from the external environment. In order to ensure reliable results, the heat generation calculated for a single cell output by the MATLAB simulation is applied to each of the six cells individually. However, due to the heat transfer between the battery components the heat generation in the neighboring cell will affect the temperature of the entire battery.

As mentioned in the previous section, heat generation mainly occurs across the electrode/electrolyte interface. Employing the MATLAB simulation of the battery cell at a constant discharge rate, the heat generation at each electrode is calculated after a specified discharge time. Using the simulation data, heat generation loads are applied across the surface area of each electrode as watts per meters squared, or to the electrolyte reservoir as watts per cubic meters [7]. Prior to the effects of heat generation, the initial temperature of the
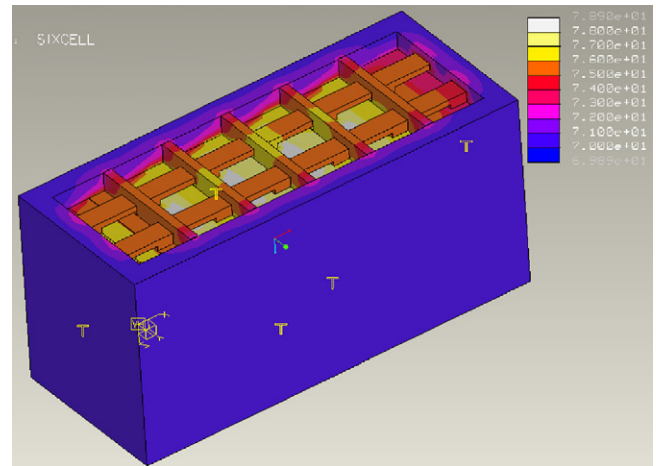
entire body is set to 300 K at each node to represent room temperature. While at low currents there is temperature variation, extreme temperatures only occur at high charge or discharge rates. As pictured below, the maximum temperatures occur in the innermost cells within the electrolyte reservoir. A significant amount of heat is transferred to the current collectors, varying only a few degrees from the cell temperature. The small variation provides evidence that due to the components thermal conductivity properties, the terminal temperatures provide a suitable approximation of internal battery temperature. Therefore, during experimentation, the temperature at the terminals will be employed to represent internal temperature for comparison with computer simulation results. Furthermore, the much safer alternative of external thermocouple readings prevents the need for thermocouple probes into the unstable battery cells.

As shown in Fig. 7, the battery casing remains at a relatively constant near room temperature throughout the discharge process. However, since the terminal temperature does not provide sufficient data to extrapolate a temperature gradient and the outer casing remains relatively consistent with ambient air temperature, a thermal imaging camera is necessary for modeling comparison.
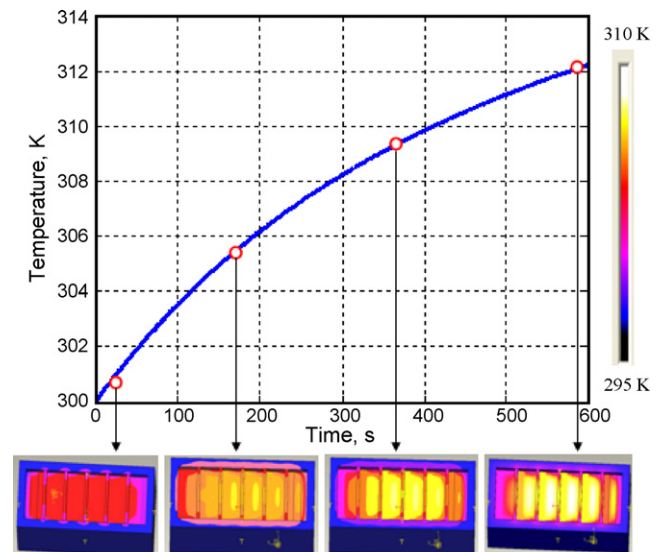

Fig. 8. Transient non-adiabatic temperature modeling comparison during the first 10 min of 60 A discharge.
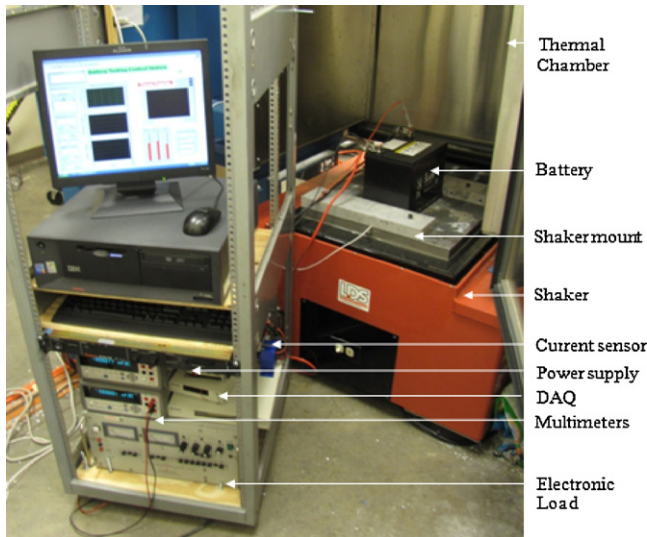
Fig. 9. Battery testing station.

Table 1
Battery data sheet.

Property	Value
Type	CMF68L
Terminals	SAE Post
Nominal voltage	12.36 V
CCA	600 A
Life cycle	4400 cycles
Reserve capacity	110 min
Charge acceptance	21 A
5 h capacity	54 A h^{-1}
Total weight	18.7 kg
Vibration test	Ok
Electrolyte specific gravity	1.26 ± 0.01

cell center. Therefore, the acid concentration will have a small but present gradient with the highest concentration experienced near the middle of the cell. Additionally, the outermost cells lower temperatures will cause a larger concentration gradient across the cell due to a decrease in particle collision. An additional side effect to the lower temperature is a slower discharge rate causing a higher voltage for the boundary cells.

The MATLAB simulation derives cell temperature as the average temperature during operation and is calculated due the change in heat transfer rate over time. For this approach, the entire cell including the electrodes and electrolyte reservoir are considered one control volume. Therefore the heat generation is applied across the entire cell equally. The temperature derived from this method is reinserted into the initial loop used to calculate reaction rate and terminal voltage. The finite element analysis applied material properties to the various components while the heat generation is applied in a similar manner to the MATLAB model.

Fig. 8 illustrates the change in temperature under 60 A discharge load for MATLAB and finite element analysis. The MATLAB simulation provides an average temperature across the cell comparable to that found using 3D finite element thermal profile. The initial temperature after only a few seconds is set prior to the simulations at 300 K, therefore the temperature is nearly identical. For the other three comparisons the MATLAB simulations shows a slightly higher temperature than that of 3D profile. The largest discrepancy occurs the longest period after the initial load is applied varying almost three degrees Kelvin. However, since battery performance changes only after significant temperature change, the small difference is acceptable.

Additionally, the comparison provides assurance that the non-adiabatic model provides a better representation of temperature change than the adiabatic case, as heat transfer with the external environment is considered for both MATLAB and finite element simulations.

4.4. Comparison with experimental data

The objective of the experimental setup is to assemble a testing environment capable of recreating battery working conditions allowing for data extraction from the important areas. A photograph of the experimental setup is provided in Fig. 9 illustrating the battery testing station during operation. The battery is placed inside the thermal chamber on the shaker platform and mounted by a wedge apparatus to ensure stabilization during vibration test-

Closer examination of Fig. 7 shows only slight variations of a couple of degree Kelvin at the center of each of the cell components. However, each of the cells experiences a significant deviation near the internal wall of the protective casing. Separation of the casing from the cells reveals a distinctive gradient for each of the battery components. The decrease in temperature towards the outer boundaries will result in a drop in reaction rate at those positions compared to the maximum temperature experienced at the
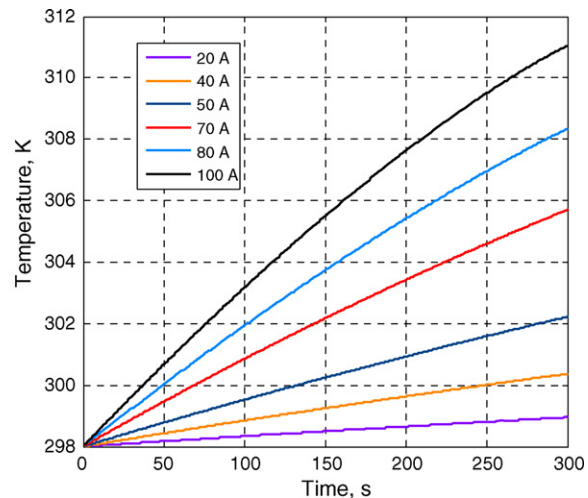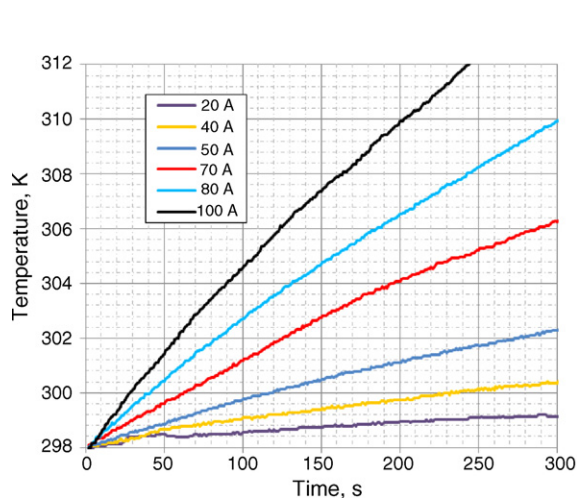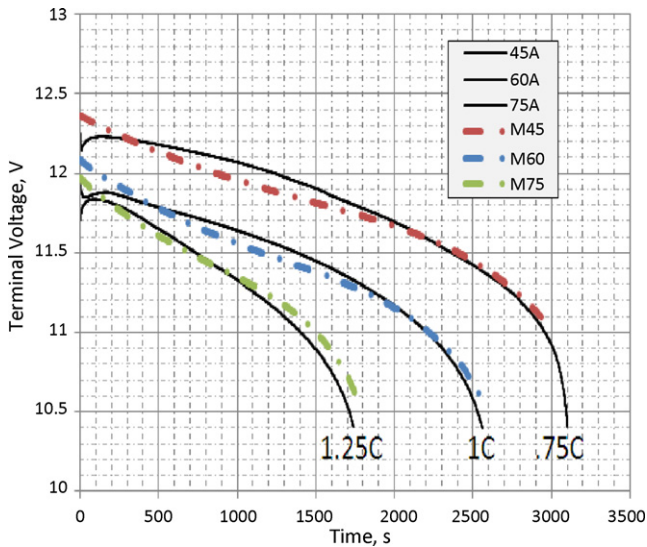

Fig. 10. Start-up behavior of temperature: (left) experiment and (right) modeling.

Fig. 11. Reference at 300 K at 100% SOC. Solid: experiment and dashed: modeling.

Fig. 13. Step response for discharge at 300 K.

ing as well as simple removal after the experiments are complete. The thermocouple wires, multimeter extensions, and battery cables are fed through a small opening in the thermal chamber floor and securely fastened to the appropriate area of the battery as shown.

The thermocouple and multi-meter measurements from the battery and the current sensor readings from the supply cable are relayed to the computer which is then organized by the LabView program created to automate the setup. Data is logged as an Excel file for future viewing and model comparison. The lead acid batteries, model CMF68L, under observation are provided by Songwoo USA Corporation. The batteries in question provide 600 Cold Cranking Amps, CCA, and have a 60 Ampere-hour capacity. Additional specifications are provided by the manufacturer are outlined in Table 1.

In order to validate the temperature change from the various sources of heat generation, thermocouples were placed on the battery terminals and casing. Reference data and comparison of experimental results to simulation outputs revealed the positive terminal as the most accurate representation of internal temperature. Initially, temperatures were gathered during the
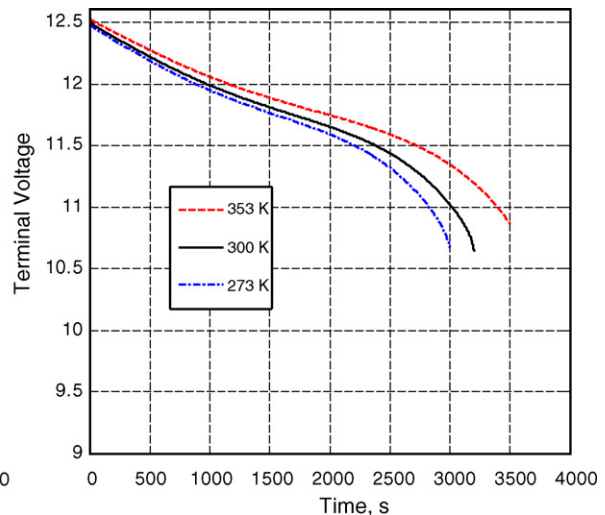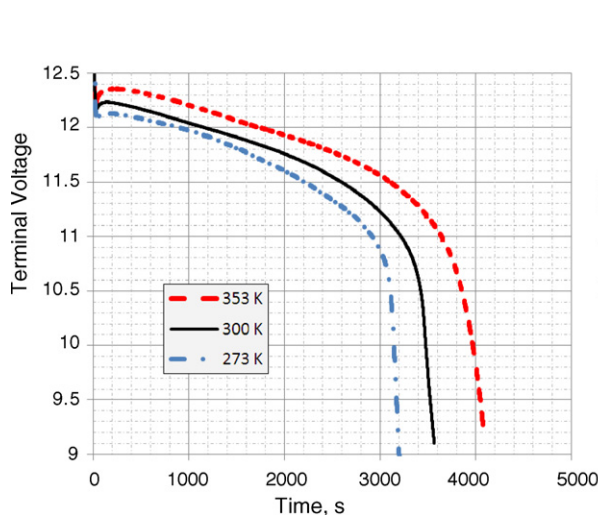
first 5 min of discharge when the greatest increase in temperature occurs. Experimental results for discharge currents ranging from 20 A to 100 A is provided in Fig. 10. MATLAB modeling of the same discharge currents is directly below the experimental results for comparison.

The temperature response of the MATLAB modeling is comparable to the readings of the strategically placed thermocouples, varying only a few degrees at high discharge currents. Additionally, the effect of heat transfer is evident as the slope of increasing temperature lessens as discharge continues for both experimental and modeling results. Therefore, non-adiabatic simulation provides a better representation of transient temperature.

4.4.1. Static and dynamic responses of terminal voltage

An example comparison of the discharge performance under the various loads at room temperature is provided in Fig. 11. Since significant heat generation only occurs under high loads, experiments involving discharge currents within the low, medium, and high ranges will be performed for comparison. The comparison provided above shows close representation by the MATLAB model of battery performance for 45 A, 60 A, and 75 A discharge at room temperature. Slight discrepancies appear for the initial voltage drop, but only vary 50 mV during the first quarter hour of discharge. There is a more significant difference near the end of discharge as the internal resistance grows causing a sudden drop in terminal voltage. The model shows similar effects from the increase in resistance but less

Fig. 12. Ambient temperature effects on terminal voltage comparison during 45 A discharge. (Left) experiment and (right) modeling.

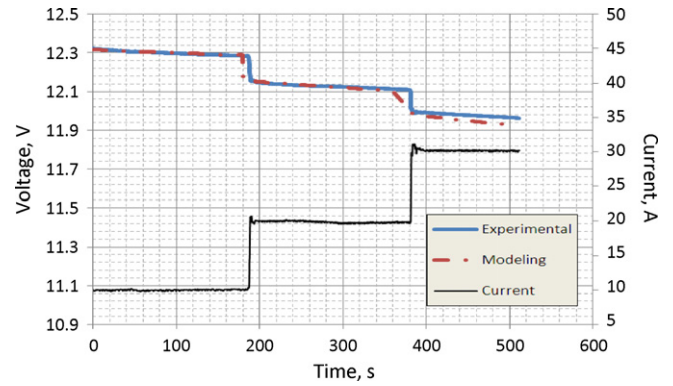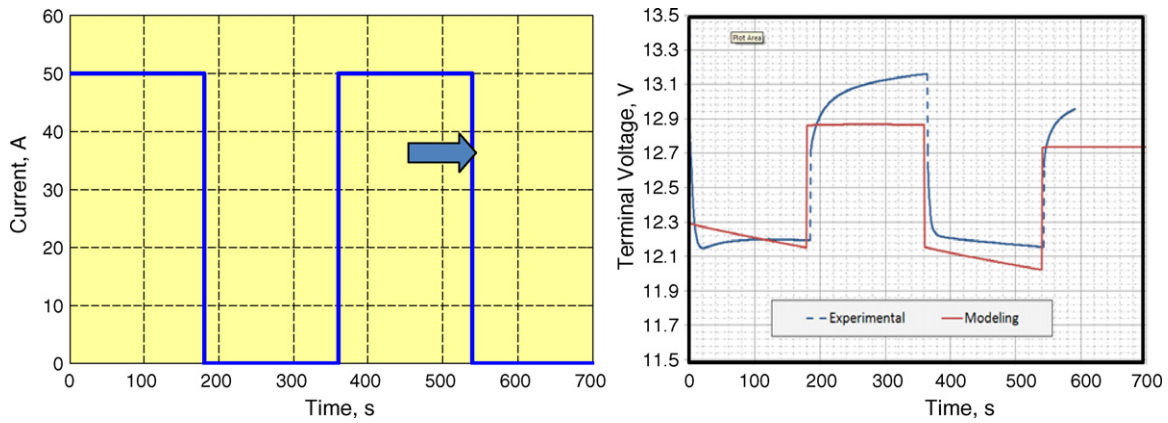**Fig. 14.** Pulse discharge response (50 A).

drastic. This is due to the model's dependence on acid concentration. As the experimental results illustrate the quick descent, the simulation is structured so that when concentration is calculated to be zero at the positive electrode the run stops, before the final drop occurs.

As experienced during the simulation of battery performance, significant change in discharge performance only occurs at extreme temperatures. The initial testing under mild conditions with minimal effects results in a reassessment of strategy focusing more intensively on the extreme temperatures and varied load responses. The remainder of the comparison of experimental results includes the reference state at 300 K, and the boundaries of the operating temperature range provided by the manufacturer of 273 K and 353 K (0 °C and 80 °C) to avoid freezing of the electrolyte. The batteries are subjected to a range of currents until near the end of discharge avoiding the final voltage drop. A comparison of experimental and simulation results are provided for 45 A discharge current at 273 K, 300 K, and 353 K, shown in Fig. 12. As illustrated above, decrease in temperature has negative effects on the battery voltage showing a slight decrease in initial voltage and significantly lower discharge time. There is about a 5 min difference in total discharge time between 273 K and 300 K, and nearly 6 min between 300 K and 353 K. The initial voltages of the plots above differ slightly due to the approximations of the initial voltage drop. However, the responses reveal similar slopes and voltage near the end of discharge. In full, the modeling shows close approximation of battery performance and the various temperatures.

Pictured below in Fig. 13 is the 10 A step input current on the right vertical axis and the response of the experimental and modeling voltage on the left hand vertical axis. Comparison of the 10 A and 20 A load steps to the modeling results shows a good relationship. However, the modeling during the 30 A load shows as much as .02 V discrepancy from the experimental data. Most notably, the initial voltage drop caused by the increase in load is greater for the modeling response while the voltage at the end of the 20 A step is slightly lower causing a compound effect. Additionally, the magnitude of the voltage drop is calculated by the product of the load current and the battery internal resistance therefore both values must be constant and accurate to provide a proper representation. Yet, the increase in current is gradual and not instantaneous, and the internal resistance is approximated.

The response of a pulse profile pictured in Fig. 14 compares experimental and modeling results for two 50 A pulses, each followed by a period of rest of the same length. The simulation closely represents the experimental results only differing 40 mV during the second pulse.

4.5. Temperature responses

Thermal imaging emerged as the best and safest alternative for internal temperature measurement. The COMPIX PC2000 thermal imaging camera is capable of snapshots every 20 s and detecting radiation in the infrared spectrum to determine temperature across its field of view, FOV.

Observation of thermal effects with the use of the thermal imaging camera provides proof that the positive terminal provides the best comparison for MATLAB simulation results for the internal battery temperature only varying a few degrees. However, since the thermal imaging results show a distinct temperature gradient the most useful comparison is with three-dimensional finite element modeling as shown in previous section. The three-dimensional FE analysis is a transient model as heat generation changes throughout the charge and discharge processes as function of overpotentials and temperature coefficients at the electrodes. As a result, snapshots from the ANSYS and ProE analysis are taken at instances consistent with the discharge time captured by the thermal camera. Temperature distribution from the modeling and experimental testing are compared below extracting results from the initial equilibrium state.

Over the duration of discharge, the magnitude of overpotential steadily decreases resulting in a noticeable decrease in slope of transient temperature. Additionally, the incorporation of heat transfer effects causes decrease in temperature as the external environment and battery work to achieve thermal equilibrium. Therefore, the first 6 min of discharge shows the greatest change in cell temperature validated by the analysis illustrated in Fig. 15. The comparison in the figure shows temperature distribution consistent with thermal imaging results. In both cases, the highest temperatures nearing 310 K after 180 s occur in the center of the battery at the top of the electrodes near the current collectors and decrease slightly in the cells near the boundaries of the outer casing. Elevated temperature in this area is a result of greater current flow through the metallic components connected to each terminal which are removed for easier view of the battery cells. The variation between the terminal temperature and internal cell temperature is a result of the contact surface area between the electrical cable connectors and the terminals. In Fig. 16, the center cells show a 310 K temperature while the outer cells experience temperatures near 300 K.
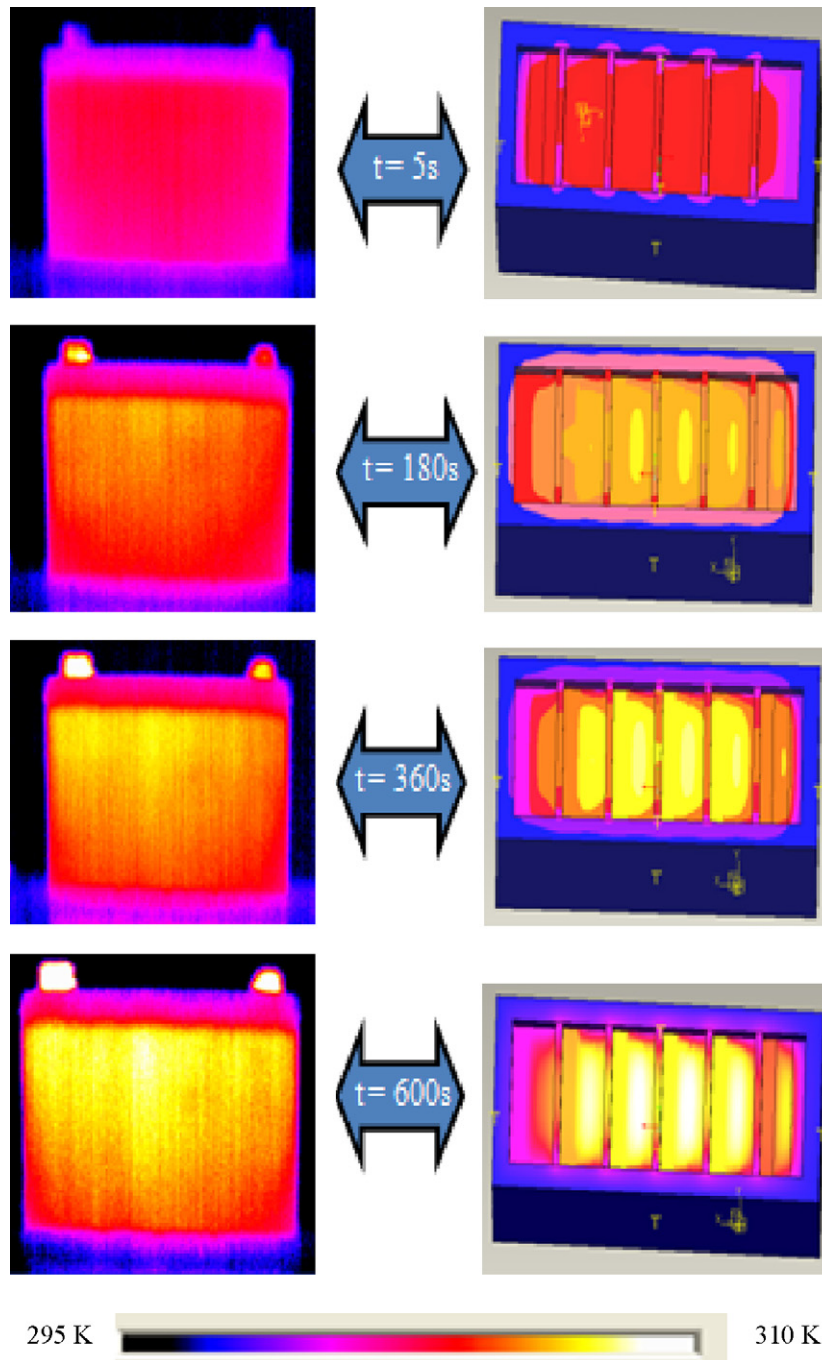
295 K ▬▬▬▬▬▬▬▬▬▬ 310 K

Fig. 15. Thermal imaging and FE analysis comparison at 60 A discharge.
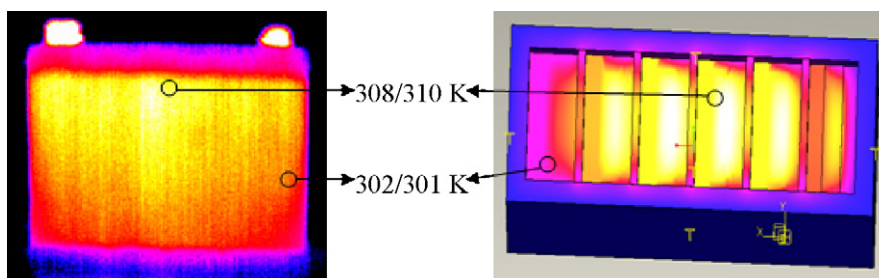

308/310 K

302/301 K

Fig. 16. Temperature comparison 600 s after 60 A load.

5. Conclusions

This paper outlines the communication of a mathematical model and finite element analysis seeking to fully represent the performance of a six cell maintenance-free lead acid battery for implementation into existing vehicle models. Following modeling results, experimental data is obtained to establish validity of the simulations. Close attention is paid to the thermal effects of the various components and electrochemical processes present in the battery cells that determine quality of performance.

Major contributions of this paper are summarized as follows:

- As expected, increase in current results in a higher reaction rate along with a greater percentage of reactions occurring along the electrode electrolyte interface. Reaction rates grow increasingly uniform across each of the electrodes for both the charge and discharge process as temperature rises due to increased ionic conductivity and diffusivity. The small gradient aids in the battery's ability to hold charge. The effect of the temperature coefficients outweigh any decrease in voltage that may be caused by a decrease in gradient.
- Significant change in voltage experienced at the terminals only resulted from temperature change of at least 10 K. Therefore, for the isothermal simulation, temperatures that varied 20 K showed obvious change which was later verified through tests. For the simulations incorporating transient heat generation, considerable temperature increase for typical battery operation only occurs at high discharge currents, 30 A and above. Consequently, isolated short pulses in HEV or SLI applications will have result in only slight temperature change.
- Examining the different causes for heat generation reveals the contribution of the reversible and irreversible processes. The irreversible effects are constantly changing throughout battery operation. As a result, the percentage of heat generation caused by overpotentials is directly dependent on the current applied. For currents below 30 A, the reversible effects are an order of magnitude higher. However, both processes exhibit comparable contributions to the overall heat generation of the system for discharge current exceeding 70 A.
- Temperature distribution from the finite element simulation is consistent with thermal imaging data gathered revealing the maximum temperature in the center of the cell slowly decreasing towards the boundaries a total of 5 K under 60 A discharge. Similar temperature distribution arose regardless of load current, only differing in magnitude.
- The thermal effects became to focal point of the remaining modeling and experimental testing. As for the modeling modifications, the maximum electrolyte concentration approximated by previous researchers did not hold true for the battery under observation. Once the maximum specific gravity was obtained from the manufacturer and the corresponding concentration calculated. Following the correction, the results were largely improved.

5.1. Further tasks

Overall, the goals set prior to modeling and experimental efforts were achieved. The modeling and experimental data provide a full representation for the specific lead acid battery under observation, also allowing for manipulation of battery parameters to simulate other battery designs. However, the overall system has a few minor shortcomings leaving room for additional testing. Namely, the MATLAB simulation is capable of calculating the SOC as a function of the applied load of a certain amount of time, but reliable approximation of battery SOC during tests is absent.

Appendix A.

Parameter	Value	Reference
Initial specific surface area for Pb electrode a_{maxPb} (cm^{-1})	23,000	[3]
Initial specific surface area for PbO$_2$ electrode $a_{maxPbO2}$ (cm^{-1})	230,000	[3]
Initial exchange current density i_{0maxPb} (A cm^{-2})	4.96×10^{-6}	[3]
Initial exchange current density $i_{0maxPbO2}$ (A cm^{-2})	3.19×10^{-7}	[3]
Pb electrode conductivity (S cm^{-1})	500	[7]
PbO$_2$ electrode conductivity (S cm^{-1})	4.8×10^4	[7]
Initial cell temperature T (K)	298	–
Ambient temperature T_a (K)	298	–
Standard reduction potential E_{Pb} (V)	−0.356	[6]
Standard reduction potential E_{PbO_2} (V)	1.685	[6]
Cathodic charge transfer coefficient α_{Pb}	.45	[3]
Anodic charge transfer coefficient α_{Pb}	1.55	[3]
Cathodic charge transfer coefficient α_{PbO_2}	.85	[3]
Anodic charge transfer coefficient α_{PbO_2}	1.15	[3]
Exponent for exchange current density ξ_{Pb}	0	[3]
Exponent for exchange current density ξ_{PbO_2}	0.3	[3]
Pb electrode size V_{Pb} (cm^3)	49	–
Pb electrode size V_{PbO_2} (cm^3)	151.9	–
Mean ionic coefficient $\gamma \pm$	Fitted from data	[1]
Specific heat capacity of electrolyte c_v (J (kg C)$^{-1}$)	Fitted from data	[1]
Temperature coefficient $\partial E_{Pb}/\partial T$ (V K^{-1})	-1.15×10^{-3}	[6]
Temperature coefficient $\partial E_{PbO2}/\partial T$ (V K^{-1})	3.27×10^{-4}	[6]
Thermal conductivity container k (W m^{-1} C^{-1})	0.2	–
Thickness of container wall ε (m)	0.005	–
Maximum electrolyte density (kg L^{-1})	1.28	–
Maximum electrolyte concentration $[SO_4H_2]_{max}$ (mol cm^{-3})	4.9×10^{-3}	–

References

[1] H. Bode, Lead Acid Batteries, Wiley and Sons, New York, NY, 1977.
[2] R. Jasinski, High-energy Batteries, Plenum Press, New York, 1967.
[3] J.J. Esperilla, J. Félez, G. Romero, A. Carretero, Journal of Power Sources 165 (1) (2007) 436–445.
[4] T.V. Nguyen, R.E. White, H. Gu, Journal of the Electrochemical Society 137 (10) (1990) 2998–3004.
[5] H. Gu, Proceedings of the Sixth Annual Battery Conference on Applications and Advances (1991) 47–56.
[6] W.B. Gu, G.Q. Wang, C.Y. Wang, Journal of Power Sources 108 (1) (2002) 174–184.
[7] W.B. Gu, C.Y. Wang, Journal of The Electrochemical Society 147 (8) (2000) 2910–2922.
[8] T.R. Crompton, Battery Reference Book, Newnes, 2000, ISBN: 0-7506-4625-x.
[9] S.-C. Kim, W.-H. Hong, Journal of Power Sources 77 (1999) 74–82.
[10] D. Baert, A. Vervaet, Electrochimica Acta 44 (1999) 3491–3504.
[11] W. Tiedemann, J. Newman, in: S. Gross (Ed.), Battery Design and Optimization, The Electrochemical Society, Princeton, NJ, 1979, pp. 39–49.
[12] Venkat Srinivasan, G.Q. Wang, C.Y. Wang, Journal of The Electrochemical Society 150 (2003) A316–A325.
[13] K.W. Morton, D.F. Mayers, Numerical Solution of Partial Differential Equations, 2nd ed., Cambridge University Press, 2005.